Tellus (1991), *43A*, 321–333

Orographic destabilization of a laterally sheared flow

By H. C. DAVIES[1] and CH. SCHÄR[2], [1]*Atmospheric Physics, ETH, Hönggerberg, 8093 Zürich, Switzerland*; [2] *Department of Geology and Geophysics, Yale University, New Haven, USA*

(Manuscript received 1 August 1990; in final form 29 January 1991)

ABSTRACT

It is shown that a topographically-induced instability can exist for a laterally sheared flow aligned along the contours of a two-dimensional ridge. The nature of the destabilization mechanism is explored within a quasi-geostrophic, f-plane framework for adiabatic flow of an incompressible stratified fluid occupying the half-space $z > 0$. For a basic state of uniform barotropic shear with (or without) the superposition of an uniform baroclinic component, the instability is shown to be engendered by the terrain shape, sustained by the lateral shear, and inhibited by the baroclinicity. A phenomenological interpretation in terms of the interaction of two "vortex-like" wave-trains located on the adjacent slopes of the terrain accounts neatly for the salient features of the instability. It is shown that there is a similar instability associated with the hybrid configuration of an enhanced baroclinic zone set alongside a terrain slope. Consideration is also given to the limitations of the diagnosed instability and to the possibility of its manifestation in various geophysical systems. In particular, it is suggested that some of the observed cyclogenetic activity along the eastern seaboard of north America and around the periphery of Antarctica could be related to terrain-induced instability effects.

1. Introduction

Atmospheric and oceanic flows can be influenced in diverse ways by variations in the height of the underlying terrain. A major factor in determining the nature of this influence is the spatial scale of the variations. If the horizontal extent of the terrain feature is large enough then the response can be quasi-geostrophic and occur predominantly in-situ above the terrain.

Here our interest is in the influence of such terrain upon the stability of the overlying flow. From this standpoint, the terrain height variations influence the structure of the basic flow and also permit orographically-induced vortex stretching effects to modify perturbations away from that state. These vortex stretching effects can act to modify an instability that would be present even in the absence of terrain variations, or serve to catalyse some other form of instability.

Theoretical studies of these possibilities have focussed on two different types of flow configurations. In one category consideration is given to the instability of a flow over longitudinally periodic terrain set on a β-plane with the basic steady state comprising a zonal flow plus a wave component. In this case the terrain can induce a wave pattern which is itself intrinsically unstable (Lorenz, 1972; Hoskins, 1973; Gill, 1974) or serve as the seat for an orographically-dependent instability (Charney and DeVore, 1979; Hart, 1979; Pedlosky, 1981; Hoskins and Revell, 1984). There can also be some combination of the foregoing (see the discussions in Källén, 1983; Frederiksen and Bell, 1987; Reinholdt, 1990).

Studies in the 2nd category consider the (often subtle) modifications of classical barotropic/baroclinic instability due to the presence of terrain variations transverse to an uni-directed basic state. For example the addition of an uniform bottom boundary slope to the standard Eady problem can, depending upon the relative values (amplitude and sign) of the terrain slope and the basic-state isentropic slope, enhance or inhibit the growth rate of the normal modes of the system (Hide, 1969; Blumsack and Gierasch, 1972). Again the results of Speranza et al. (1985) indicate that for an elongated ridge the terrain inhibits somewhat the Eady instability as well as introducing notable structural changes to the most unstable mode.

Sinusoidal cross-stream topography not only modifies the Eady modes but also catalyses a hybrid type of instability (DeSzoeke, 1975). Studies of the foregoing kind have also been undertaken for the β-plane, two-layer variant of the classical baroclinic instability problem (e.g., Orlanski, 1969; Orlanski and Cox, 1973; Davies, 1975; Durney, 1977; Mechoso and Sinton, 1981; De Szoeke, 1986).

In the present study, we consider an orographically catalysed destabilization (c.f., the 1st category) of a basic flow that is directed along a ridge (c.f., the 2nd category). However in contrast to both of the foregoing categories the instability will be shown to be associated intrinsically with the lateral shear at low-level. The possibility for such an instability was noted by Pedlosky (1980). He ascertained the form of the neutral wave and explored the nature of the contiguous unstable modes for one particular terrain configuration comprising a combination of linear and quadratic height contributions. Here in the framework of quasi-geostrophic theory a fuller examination is undertaken of the properties and nature of this instability for a locally confined topographic feature. The approach is to perform a normal mode analysis and to provide a phenomenological interpretation. Possible extensions to, and limitations of, the study are also discussed, and some consideration given to the relationship of the theory to observed phenomena.

2. The model system

2.1. The governing equations

We restrict ourselves to consideration of the quasi-geostrophic flow of an incompressible fluid that occupies the half-space $z>0$ of an f-plane. The medium is taken to have an uniform background stratification (N) and uniform relative potential vorticity (Λ). In this limit the linear equations governing small amplitude perturbations of the system for a basic state $\bar{U}=\bar{U}(y,z)$ that is aligned parallel to the terrain, $\bar{h}=\bar{h}(y)$, comprise: the perturbation potential vorticity equation,

$$\left[\frac{\partial}{\partial t}+\bar{U}\frac{\partial}{\partial x}\right]\left(\frac{\partial^2\psi'}{\partial x^2}+\frac{\partial^2\psi'}{\partial y^2}+\frac{f^2}{N^2}\frac{\partial^2\psi'}{\partial z^2}\right)=0, \qquad (2.1)$$

with the boundary conditions given by:

– the thermodynamic equation applied at the level $z=0$,

$$\left[\frac{\partial}{\partial t}+\bar{U}\frac{\partial}{\partial x}\right]\left(\frac{g\theta'}{\Theta}\right)+v'\frac{\partial}{\partial y}\left(\frac{g\bar{\theta}}{\Theta}\right)+w'N^2=0, \qquad (2.2a)$$

where

$$w'=v'\frac{\partial\bar{h}}{\partial y}; \qquad (2.2b)$$

a far-field stipulation consistent with the perturbations being "bottom-confined" i.e.,

$$\psi'\to 0 \qquad \text{as} \quad z\to\infty. \qquad (2.3)$$

For ease of reference we shall identify the y-axis as pointing "northward". The remaining notation is conventional with (ψ',θ') signifying the perturbation fields of the streamfunction and the potential temperature, whilst $\bar{\theta}=\bar{\theta}(y)$ refers to the deviation of the mean thermal state away from that of the uniform background stratification. It follows that

$$\left(\frac{g\theta'}{\Theta}\right)=f\frac{\partial\psi'}{\partial z}, \qquad (2.4a)$$

and

$$f\frac{\partial\bar{U}}{\partial z}=\frac{\partial}{\partial y}\left(\frac{g\bar{\theta}}{\Theta}\right). \qquad (2.4b)$$

2.2. General instability criteria

Integral relationships for perturbations of this system (i.e., eqs. (2.1)–(2.3)) for the basic state $\bar{U}=\bar{U}(y,z)$ take the form (c.f., Schär and Davies, 1990):

$$\frac{\partial}{\partial t}\left\{\int_x\int_y \mathscr{R}\,\mathrm{d}x\,\mathrm{d}y\right\}=0, \qquad (2.5)$$

and

$$\frac{\partial}{\partial t}\left\{\int_x\int_y U\mathscr{R}\,\mathrm{d}x\,\mathrm{d}y\right\}\geqslant 0, \qquad (2.6)$$

where

$$\mathscr{R} = \left(\frac{N^2}{f}\frac{\partial \bar{h}}{\partial y} - \frac{\partial \bar{U}}{\partial z}\right)\frac{1}{2}\eta'^2,$$

$$= \frac{1}{f}\frac{\partial \bar{R}}{\partial y}\frac{1}{2}\eta'^2, \quad \text{with } \bar{R} = N^2\bar{h} - \left(\frac{g\bar{\theta}}{\Theta}\right). \tag{2.7}$$

The surface integral is taken over the entire lower boundary of the flow domain, η' denotes the perturbation displacement in the across-stream direction, and the expression for $\bar{R}$ was derived using the thermal wind relationship (2.4b). Note that the derivative $(\partial \bar{R}/\partial y)$ is proportional to the difference in the across-stream gradient of the terrain slope and the basic state isentropic slope, and hence positive and negative extrema of $\bar{R}$ correlate with corresponding extrema in the potential temperature at the surface $z = \bar{h}(y)$.

In the context of flow stability the stipulation that the flow is of uniform potential vorticity (PV) and semi-infinite in extent implies that the dynamics of this simplified system is such that the vertical structure of the perturbated flow is evanescent (c.f., 2.3) and the conventional variants of barotropic-baroclinic instability are specifically excluded. Thus any remaining instability of the system must be related to surface thermal effects and/or terrain effects. The significance of the integral constraints (2.5–2.6) can be illustrated as follows: the growth of small perturbations requires that the variance of η' at the surface must increase with time and this is only possible for a basic state flow characterized by a local surface maximum (minimum) of $\bar{R}$, together with a basic state of positive (negative) lateral shear. Thus, in the presence of an appropriate lateral shear of the basic state, there are three physically distinct configurations that are potentially unstable: a thermal extremum in the absence of topography; a terrain extremum in a purely vertically stratified medium; a suitable hybrid combination of monotonic terrain and thermal variations that together yield an extremum of $\bar{R}$. The first configuration was examined by Schär and Davies (1990) in the context of the generation of frontal wave cyclones and the second was the subject of Pedlosky's (1980) study.

2.3. *The basic state*

In line with the prescribed stipulations for our system the unperturbed state is taken to be a basic flow of uniform barotropic shear either with, or without, an accompanying uniform baroclinic component. Further the flow is taken to be aligned along the contours of a two-dimensional "Witch of Agnesi" ridge,

$$\bar{h} = \frac{\bar{h}_m}{[1 + (\bar{y}/a)^2]} \tag{2.8}$$

Table 1. *List displaying the spatial and velocity scales adopted for the non-dimensionalization of the instability problem together with the implied scales for time, temperature, pressure and vorticity; also listed for illustrative purposes are three possible atmospheric settings*

Dimensionless notation		Possible atmospheric settings			
		setting I	setting II	setting III	setting IV
horizontal scale	a	400 km	200 km	100 km	200 km
velocity scale	U	20 m/s	10 m/s	5 m/s	5 m/s
Rossby-number	U/af	0.5	0.5	0.5	0.25
time scale	a/U	5.6 h	5.6 h	5.6 h	11.1 h
temperature scale	$UN\Theta/g$	5.6 K	2.8 K	1.4 K	1.4 K
pressure scale	$aUf\rho_0$	8 hPa	2 hPa	0.5 hPa	1 hPa
vorticity scale*	$R_0 f$	0.5 f	0.5 f	0.5 f	0.25 f
mountain height	$F^{-1} = 1.0$	2000 m	1000 m	500 m	500 m
mountain height	$F^{-1} = 2.0$	4000 m	2000 m	1000 m	1000 m
mountain height	$F^{-1} = 2.5$	5000 m	2500 m	1250 m	1250 m
mountain height	$F^{-1} = 3.0$	6000 m	3000 m	1500 m	1500 m
temp. gradient	$F_{ut} = 0.5$	0.7 K/100 km	1.4 K/100 km	0.7 K/100 km	0.35 K/100 km
temp. gradient	$F_{ut} = 1.0$	1.4 K/100 km	2.8 K/100 km	1.4 K/100 km	0.7 K/100 km

The system is non-dimensionalized (see Table 1) in terms of length and velocity scales based respectively upon the mountain half-width (a) and a velocity scale U corresponding to the amplitude of the basic state velocity at $(a, 0)$, i.e., $U = \Lambda a$. In this non-dimensional frame the basic state geostrophic stream function and velocity take the forms,

$$\hat{\bar{\psi}}(\hat{y}, \hat{z}) = \tfrac{1}{2}F_r(\hat{y}^2 - \hat{z}^2) - F_{ut}\hat{y}\hat{z}, \tag{2.9}$$

$$\hat{\bar{U}}(\hat{y}, \hat{z}) = -F_r\hat{y} + F_{ut}\hat{z}. \tag{2.10}$$

Here the caret symbol signifies a non-dimensional variable, and the overbar refers to the mean state. The crest height of the ridge ($\bar{h}_m$) is defined in terms of an inverse Froude number,

$$F^{-1} = (Nh_m/U).$$

The parameter F^{-1} is a measure of the terrain height for a fixed value of the shear (or an inverse measure of the shear for a specified mountain height), whilst F_{ut} denotes the non-dimensional amplitude of the baroclinic component. In this dimensionless framework, the amplitude of the barotropic component is by definition scaled to unity (i.e., $F_r = 1$), and thus the flow stability is a function of the two parameters (F^{-1}, F_{ut}). Table 1 provides a full listing of the dimensionalization (also listed for use later are examples of various conceivable "atmospheric" settings for the orography and the flow field).

3. Mathematical and physical analysis of the instability

3.1. Normal mode analysis

A stability analysis of the "ridge-flow" problem posed in the previous section is undertaken following the procedure adopted by Schär and Davies (1990). The perturbation fields are assigned a single wave component, k, in the along ridge direction and a spectral representation in (y, z), so that for example:

$$\theta'(x, y, z) = [\Sigma_l P_l(t)\, e^{-\mu_l z} e^{im_l y}]\, e^{ikx}. \tag{3.1}$$

Here $m_l = (2\pi l/L_y)$ where L_y denotes the width of the computational domain in the y-direction, with $\mu_l = (k^2 + m_l^2)^{1/2}$ and $P_0 = 0$.

Note that: the adoption of an unbounded atmosphere of uniform potential vorticity constraints the perturbations to take on an evanescent structure in the vertical; the representation (3.1) presumes a lateral boundary condition of periodic continuation in the y-direction, and for physical credence, this requires the amplitude of the perturbation to be small near the boundaries (a feature that is verified a posteriori).

The series (3.1) for the perturbation field is truncated with, typically, 64 spectral components. On substitution in (2.2) it yields a set of linear differential equations for the amplitudes P_l. The fastest growing normal mode for each prescribed along-ridge wavenumber (k) is then determined using an initial-value technique. Details of the numerical procedures can be found in Schär and Davies (1990).

The growth rate spectra derived for the barotropic problem ($F_{ut} = 0$) are shown in Fig. 1 for flow settings corresponding to $F^{-1} = 2.0$, 2.5, and 3.0. Within this range the growth rate of the most unstable mode is comparatively insensitive to an increase in the value of F^{-1}, whereas there is a significant increase of its wavenumber. It also follows, since the amplitude of the lateral shear provides the time-scale for the non-dimensionalization, that it is essentially the value of this shear component that establishes the amplitude of the growth rate.

Fig. 2 shows the corresponding spectra obtained for a barotropic-cum-baroclinic basic state. Results are shown for flow configurations corresponding to a fixed value of the mountain height ($F^{-1} = 2$) and three different values of the basic state baroclinicity ($F_{ut} = 0.0$, 0.5, 1.0). The presence of the background baroclinic field is seen to inhibit

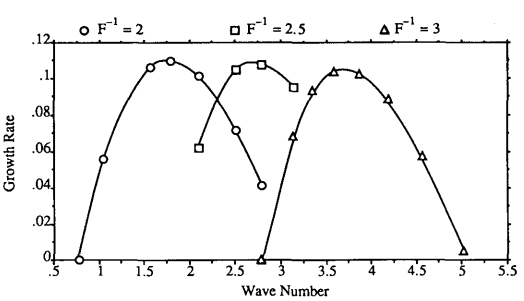

Fig. 1. Growth rate spectra for the case of along-ridge barotropic shear flow displayed for various values of the dimensionless mountain height ($F^{-1} = 2.0$, 2.5, 3.0).

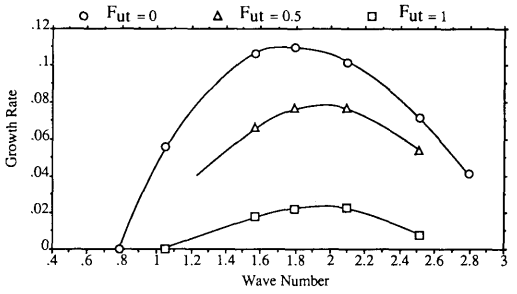

Fig. 2. Growth rate spectra for the case of uniform barotropic and baroclinic flow displayed for a fixed value of the dimensionless mountain height ($F^{-1} = 2$), and various values of the baroclinicity ($F_{ut} = 0.0, 0.5, 1.0$).

the instability without inducing a significant change in the wavelength of the most unstable mode. (A further slight increase of the baroclinicity beyond $F_{ut} = 1.0$ quenches the instability.) Table 2 provides a summary of the characteristics of the most unstable modes displayed in Figs. 1 and 2.

An indication of the spatial structure of these most unstable modes is given in Fig. 3 for the barotropic cases of $(F^{-1}) = (2.0$ and $3.0)$. The successive panels depict the surface distribution of the perturbation fields of the potential temperature, pressure and vorticity—recall that for these surface-confined modes, the vertical structure is evanescent (see 3.1) and that the vertical decay rate is inversely related to the characteristic horizontal length scale of the perturbation. The panels reveal a double wave train arranged in quadrature astride the ridge and this structure is consistent with the instability being another variant of the so-called interaction effect of two vortex-like wave-trains (c.f., Hoskins et al., 1985; Schär and Davies, 1990).

Fig. 4 is an analogous diagram for two mixed barotropic-baroclinic situations corresponding respectively to the parameter settings of $(F^{-1}, F_{ut}) = (2.0, 0.5)$ and $(2.0, 1.0)$. The baroclinicity is seen to break the across-ridge symmetry of the pattern such that the axis of zero thermal perturbation is displayed slightly southward. The northern wave train is enhanced in amplitude and enlarged in its lateral scale whereas the reverse applies to the southern train.

Table 2. *A list of various flow settings, (F^{-1}, F_{ut}), for which a normal mode analysis has been undertaken together with a catalogue for each setting of the properties of the most unstable mode*

Flow setting		Most unstable mode			
F^{-1}	F_{ut}	wave number	wave length	growth rate	doubling time
2	0	1.795	3.5	0.1095	6.3
2.5	0	2.793	2.25	0.1078	6.4
3	0	3.590	1.75	0.1037	6.7
2	0.5	2.094	3.0	0.0766	9.0
2	1.0	2.094	3.0	0.0230	30.1

3.2. A phenomenological interpretation

A helpful phenomenological interpretation of the instability can be gained by regarding the individual neighbouring wave-trains located on the adjacent northern and southern slopes of the terrain (see Fig. 3) to be topographic-Rossby waves. The difference in sign of $(\partial \bar{R}/\partial y)$ on these slopes implies that the intrinsic phase velocities of the wave-trains are directed in opposite directions. The ensuing "instability-picture" is that the difference in the strength of the ambient "local" mean flow on the two slopes can counteract the differential phase effect, hold the wave-trains stationary relative to one another, and concomitantly allow them to grow at the expense of the kinetic energy of the mean flow. Here we develop this interpretation further to account qualitatively for salient features of the instability.

Case (a): Uniform barotropic shear

Consider two perturbation wave-trains aligned as sketched in Fig. 5. Each of the wave trains $(W_I, C_I, \ldots)$ and $(W_{II}, C_{II}, \ldots)$ is taken to be composed of alternate isolated warm and cold thermal anomalies that possess characteristic dimensions in the along- and across-ridge directions of respectively $\mathscr{L}$ and $\mathscr{d}$. These anomalies are regarded as the result of alternately directed, lateral displacement of fluid bands on each slope. Our objective is to *estimate* the self-induced phase speed of each wave-train and the growth rate of the anomalies. (To facilitate identification of the underlying physical processes, we revert here to operating with dimensional variables.)

For our linear system (i.e., eqs. (2.1)–(2.3)) the

Tellus A/43/5-5

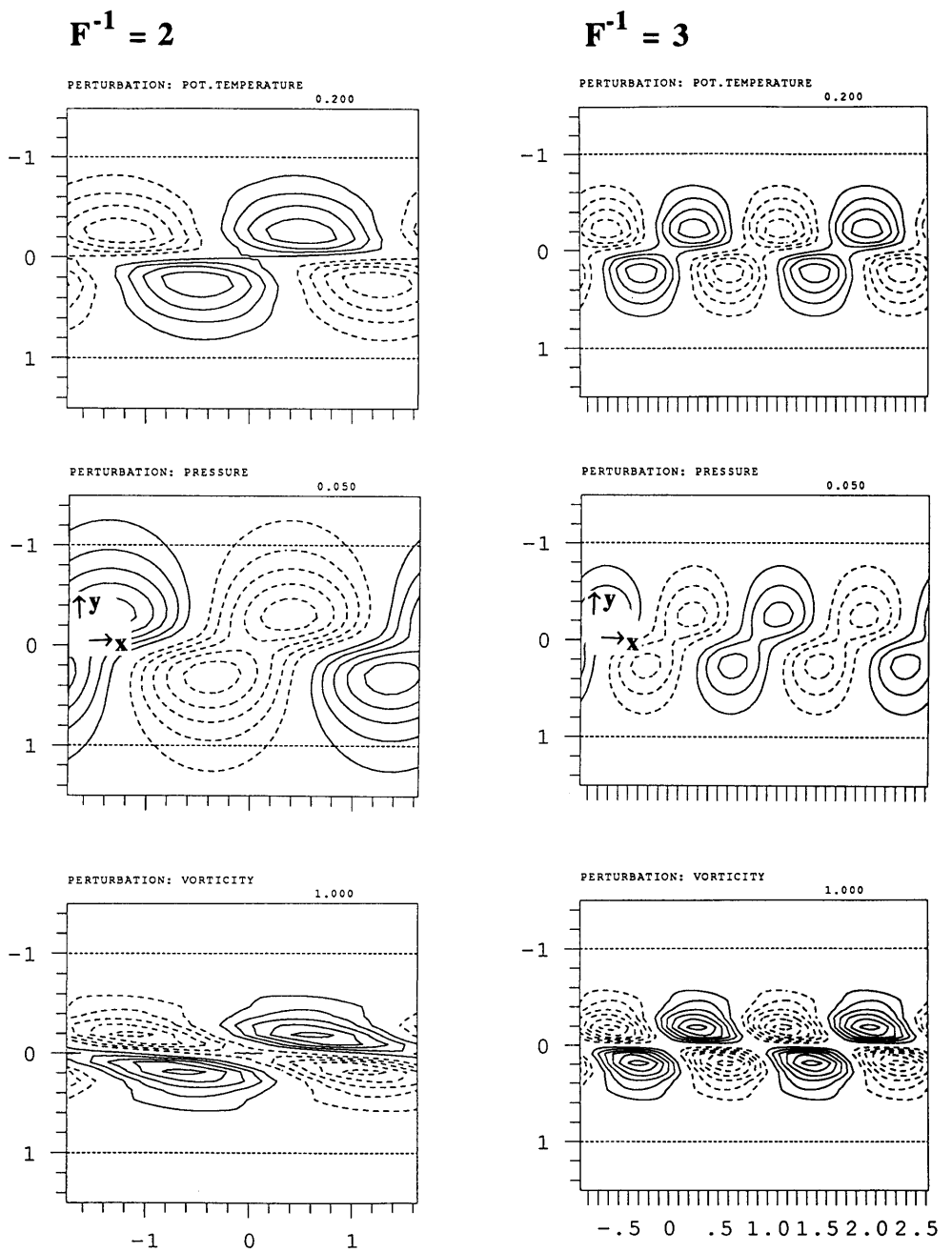

Fig. 3. Surface structure of the potential temperature (upper panels), pressure (middle panels), and relative vorticity (lower panels) for the most unstable modes of uniform barotropic flow ($F_{ut} = 0$). The results are for the two settings corresponding to the dimensionless mountain heights of $F^{-1} = 2.0$ (left panels) and $F^{-1} = 3.0$ (right panels). The amplitude of the thermal perturbation has been normalized to unity. Note that the dimensionless isoline spacing is indicated by the number at the right-hand corner of each panel, negative contours are dashed, and the zero-contour has been suppressed.

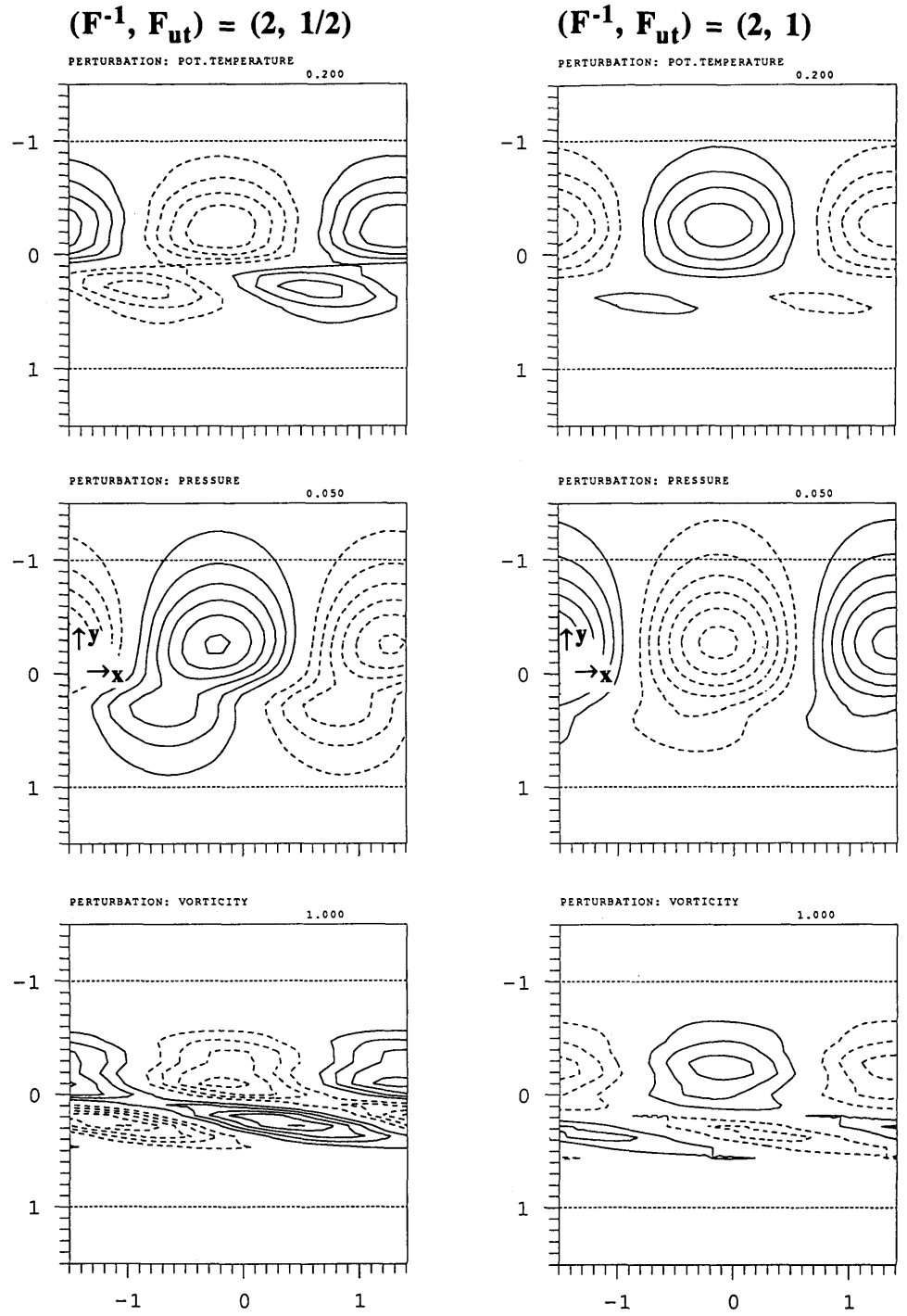

Fig. 4. As for Fig. 3 but for the two mixed barotropic-baroclinic flow settings of $(F^{-1}, F_{ut}) = (2.0, 0.5)$ and (2.0, 1.0).

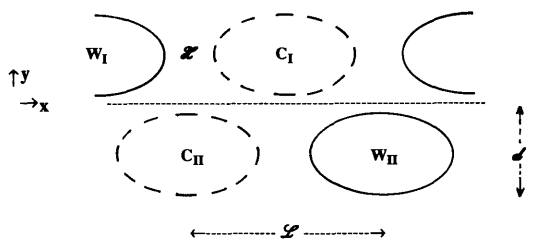

Fig. 5. Schematic of two perturbation wave-trains with each composed of alternate isolated warm and cold anomalies of dimension $\mathscr{L}$ and $\mathscr{d}$.

amplitudes of the thermal perturbation and the displacement are such that,

$$\frac{\partial \psi'}{\partial z} = \eta' \left[\frac{\partial \bar{U}}{\partial z} - \frac{N^2}{f} \frac{\partial \bar{h}}{\partial y} \right], \tag{3.2}$$

and the stream function field at the indicated point $\mathscr{H}$ in Fig. 5, due to the surface thermal anomalies, is (from the Green's Function formula),

$$[\Psi']_{\mathscr{H}} = -\frac{1}{2\pi} \frac{f}{N} \int_{s'} \frac{\partial \psi'}{\partial z} [|\boldsymbol{r} - \boldsymbol{r}'|^2]^{-1/2} \, \mathrm{d}s', \tag{3.3}$$

where $\boldsymbol{r}$ and $\boldsymbol{r}'$ are the position vectors relative respectively to the origin and the point $\mathscr{H}$ and the integral is over the surface S.

Also note that co-inspection of Figs. (1, 2 and 5) indicates that $(\mathscr{d}/a) \ll 1$. It then follows from (2.8) that

$$\left(\frac{\partial \bar{h}}{\partial y} \right)_{y = (1/2)\mathscr{d}} \approx \left(\frac{h_m}{a} \right) \left(\frac{\mathscr{d}}{a} \right). \tag{3.4}$$

Consider first the propagation speed of the wave-trains. On the basis of eqs. (3.2–3.3) a *crude* estimate of the northward-directed velocity at the point $\mathscr{H}$ due to the thermal anomalies W_I and C_I is,

$$[v']_{\mathscr{H}} \approx \frac{8}{\pi} \eta' N \left(\frac{\partial \bar{h}}{\partial y} \right)_{y = (1/2)\mathscr{d}} \left(\frac{\mathscr{d}}{\mathscr{L}} \right). \tag{3.5}$$

Thus after a time, $\approx \eta'/v'$, a new warm anomaly of amplitude comparable to W_I will form at $\mathscr{H}$. This and the formation of attendant neighbouring cold anomalies etc. constitutes in effect to an eastward propagation of the wave-train by 1/4 of the wavelength $\mathscr{L}$. Thus an approximate measure of the self-induced phase-speed, c, of the northerly wave-train is,

$$c \approx \frac{1}{4} \mathscr{L} \frac{v'}{\eta'},$$

and hence it follows from the foregoing that,

$$c \approx N h_m \left(\frac{\mathscr{d}}{a} \right)^2. \tag{3.6}$$

For the wave-trains to be stationary relative to one another symmetry considerations imply that the self-induced phase-speed be offset by the mean flow at $y = \pm \langle 1/2(\mathscr{d}) \rangle$, i.e.,

$$\langle c \rangle = \langle (\tfrac{1}{2}) \Lambda \mathscr{d} \rangle.$$

This leads directly to the relationship,

$$\left(\frac{\mathscr{d}}{a} \right) \approx \pi / (4F^{-1}). \tag{3.7}$$

Now we seek an estimate for the doubling time of the north-south displacement amplitude of the wave-trains. To this end consider first the northward-directed velocity v_0 at the centre (O) of the anomaly C_{II} due to flow fields associated with the anomalies W_I and C_I of the northerly wave-train. From (3.2–3.3) an approximate measure of this velocity is,

$$v_0 \approx \frac{2}{\pi} \eta' N \left(\frac{\partial \bar{h}}{\partial y} \right)_{y = (1/2)\mathscr{d}} \Phi,$$

where

$$\Phi = \frac{(4\mathscr{d}/\mathscr{L})^2}{[1 + (4\mathscr{d}/\mathscr{L})^2]^{3/2}}. \tag{3.8}$$

Thus an estimate of the time (τ) required to double the initial displacement η' at O is,

$$\tau^{-1} \approx v_0 / \eta',$$

and from (3.4, 3.7, and 3.8) we have that,

$$\tau^{-1} \approx \left(\frac{U}{a} \right) \Phi. \tag{3.9}$$

Significant deductions follow directly from relationships (3.7) and (3.9). Relationship (3.7)

indicates that the lateral scale, $(\mathscr{d}/a)$, of the perturbation is inversely proportional to (F^{-1}), a feature in harmony with the corresponding numerically computed results for the normal modes (see Fig. 3). An interpretation follows on noting that to offset, say, a moderate increase in the barotropic shear (i.e., effectively a decrease in F^{-1}) there needs to be a related increase in the propagation velocity, c. This can be achieved by centring the wave-train over steeper sloping terrain, i.e., at somewhat larger values of $(\mathscr{d}/a)$.

Again from (3.9) we deduce that the geometry of the wave-train with the fastest growth rate is set by the extremum in Φ so that,

$$\mathscr{L} \approx 4\sqrt{2}\,\mathscr{d}, \tag{3.10}$$

i.e., the kinematics of the anomaly-induced flow is such that the north-south directed velocity component, v_0, is maximized for this particular geometry. This can be understood on noting that, for a given $\mathscr{d}$ and along ridge separation $(\mathscr{L})$ of the anomalies, the factors

$$(\mathscr{d}^2 + \mathscr{L}^2)^{-1/2} \quad \text{and} \quad (\mathscr{d}/\mathscr{L})$$

influence respectively the amplitude and the direction of the induced flow component.

Thus the scale of *the most unstable wavelength* is established by the value of $\mathscr{d}$ and this in turn is set by the phase-speed constraint (3.7). The relationship (3.10) is qualitatively verified by the results portrayed in Fig. 1. A measure of the growth of this mode follows from (3.9),

$$\tau^{-1} \approx 1.8\left(\frac{U}{a}\right),$$

or

$$\tau^{-1}/f \approx 1.8R_0. \tag{3.11}$$

Thus the amplitude of the doubling time is set by the strength of the barotropic shear (or in non-dimensional terms by the value of the Rossby Number). This inference is also in reasonable accord with the results recorded in Table 2.

The foregoing phenomenologically based argument and deductions although crude account neatly for, and provide useful insight to, the salient geometrical and dynamical features of the instability. As such they constitute an useful complement to the normal-mode analysis.

Case (b): Uniform barotropic and baroclinic shear

Our previous consideration of the general stability criteria (see Section 2) indicates that when there is a *surface* temperature variation in the flow specification it is the *topography* of $\bar{R}$, and not that of $\bar{h}$, that determines the characteristic of the instability. Here, we outline in general terms the influence of uniform baroclinicity upon the instability.

First note that the baroclinicity establishes an asymmetric profile of $\bar{R}$ and that the axis of the zero thermal perturbation must again be located at the extremum in the $\bar{R}$ topography. For weak positive baroclinic shear this implies that the zero line is shifted slightly southward of the *orographic* crest. Thus compared with the purely barotropic case, there is a broader and stronger negative slope of $\bar{R}$ for the northerly wave-train and a narrower and gentler positive slope for the southerly wave-train. The resulting norther and southern wave-trains are (see Fig. 4) respectively "broader (width, say $\mathscr{d}_1$) and stronger" and "narrower (width, say $\mathscr{d}_2$) and weaker". Nevertheless, they can be stationary relative to one another provided they are embedded in appropriate ambient flow fields, and moreover the southward shift of the zero-line is compatible with this requirement. However, an extension of the previous phenomenological interpretation to the present case indicates that the doubling time is modified by a factor that is proportional to

$$(\mathscr{d}_1\mathscr{d}_2)/(\mathscr{d}_1^2 + \mathscr{d}_2^2),$$

and in effect the growth rate is diminished. Indeed strong baroclinicity will eliminate the domain of the southerly wave-train (i.e., force $\mathscr{d}_2 \to 0$) and hence concomitantly shut off the instability.

Case (c): The hybrid configuration

Three distinct potentially unstable flow configurations were identified in Subsection 2.2. The results derived here and in Schär and Davies (1990) indicate that in the first two cases the instability is linked to the interaction of wave-trains located on either side of an extremum in $\bar{R}$.

A similar interpretation can be invoked for the third physically distinct, but dynamically similar,

situation of a hybrid extremum of $\bar{R}$ formed by a combination of terrain and surface thermal variations. Thus, whereas a strong uniform baroclinicity inhibits the terrain-induced instability, a localised negative (positive) extremum of baroclinicity adjacent to a positive (negative) terrain slope can destabilize the flow in the presence of a negative (positive) lateral shear. In this case the growth rate will be proportional to the product of the terrain slope and the local extremum of the baroclinicity.

4. Discussion

Our objective in the previous sections was to establish the quintessential features of a terrain-induced flow instability. This was done by adopting a quasi-geostrophic framework, prescribing a simple flow configuration for the basic state, and excluding a priori other geostrophic instabilities. Here we consider possible generalizations of the results to other flow systems, discuss the limitations imposed by the constraints, and comment upon the possible realization of the instability.

4.1. Other model systems

Both the mathematical analysis and physical interpretation of the instability were based upon quasi-geostrophic dynamics. However, the results derived in Subsection 3.1 also apply to semi-geostrophic flow, provided that the basic state is assigned an additional component of constant potential vorticity equivalent to, $\tilde{\bar{\psi}} \propto Y^2$, where Y is the geostrophic coordinate, $Y=(y-u_g/f)$. Alternatively the mountain height must be suitably rescaled).

To assess the implications of this extension of the analysis note that: the vorticity in physical space is given by $\xi/(f-\xi)$, where ξ is the transformed space vorticity; the width of the mountain in physical space has to be scaled down by the factor $[1+\xi/(f-\xi)]^{-1}$. These stipulations together with the characteristic space and time scales of the most unstable modes (see (3.7), (3.10) and (3.11)) will indicate whether prescribed flow configurations are within the limit of validity of balanced flow systems.

Another fluid system that could permit the terrain-induced instability is that of the balanced shallow water flow. Conditions compatible with such a flow limit can prevail during some seasons both in coastal regions and in large lakes.

4.2. Relationship to other processes and instabilities

In Section 3, the terrain-induced instability was examined for a highly idealised configuration. In particular the realizability of the initial flow state was not considered, the influence of dissipative boundary layer effects was neglected, other forms of instability were specifically excluded, and the finiteness of geophysical terrain ridges ignored. Here we comment in turn upon these caveats.

The envisaged basic state is of flow along the topographic contours of an elongated ridge. If such a flow is to be the result of an incident stream splitting around the ridge then dynamical constraints indicate that the upstream state must be such that $F^{-1}>1$ (see e.g., Davies and Horn, 1988; Thorsteinsson, 1988). An alternative, particularly in the context of the hybrid configuration is that the flow circumscribes a topographic feature.

In connection with dissipative effects, note that the evanescent vertical length scale, $\mathscr{D}$, of the terrain-induced perturbations is such that

$$\mathscr{D} \approx \frac{1}{2\pi}\frac{f}{N}\mathscr{d}.$$

The role of boundary layer processes needs therefore to be considered if $\mathscr{D}$ is comparable to or less than the depth of the boundary layer, and/or the doubling time scale of the instability is not much greater than the dissipative time scale.

Again, if the terrain instability is to be manifest in an essentially unmodified form within a more general flow setting then it should at least possess a faster growth rate than that associated with other potential instabilities, and its vertical evanescent scale should be considerably less than the fluid depth. To aid the assessment of these constraints, Table 3 records the doubling time (τ), the horizontal wavelength ($\mathscr{L}$) and the vertical scale ($\mathscr{D}$) of the most unstable mode of the terrain instability and the corresponding values that pertain for the Eady baroclinic instability and quasi-barotropic instability associated with a localised PV maximum. Cursory estimates based upon the displayed formulae confirms that for typical atmospheric

Table 3. *Estimates of the doubling time* (τ), *the horizontal wavelength* ($\mathscr{L}$), *and the vertical depth/depth scale* ($\mathscr{D}$) *associated with terrain-induced instability, classical Eady Instability and the quasi-barotropic instability due to a local PV maximum*

	Terrain instability	Eady instability	Quasi-barotropic instability
τ^{-1}	$\approx\left(\frac{U}{a}\right)\Phi$	$\approx\frac{f}{N}\frac{\partial \bar{U}}{\partial z}\Phi$	$\approx\bar{q}_y D_2\frac{N}{f}\Phi$
$\mathscr{L}$	$\approx\sqrt{2}\,\pi a F^{-1}$	$\approx 4\frac{N}{f}D_1$	$\approx 4\sqrt{2}\,b$
$\mathscr{D}$	$\approx\frac{1}{8}\frac{f}{N}aF^{-1}$	$\approx D_1$	$\approx\frac{1}{2\pi}\frac{f}{N}b$

Here, $\Phi\approx 2/(3\sqrt{3})$, D_1 is the separation distance of the two horizontal bounding surfaces in the Eady problem, and $(\bar{q}_y, b, D_2)$ denote respectively the horizontal gradient, the half width, and the vertical depth of the potential vorticity anomaly in the quasi-barotropic case.

and oceanic values, these constraints are certainly attainable. Note, however, that to permit a normal mode type of development, the finite length of the terrain (L_m) needs to be long relative to the wavelength of the most unstable wave, i.e.,

$$(L_m/a)\gg\sqrt{2}\,\pi F^{-1}.$$

A more general caveat to our analysis is the restriction to consideration of only normal modes. No systematic study of the initial-value problem was undertaken here but our technique for determining the normal modes did provide some evidence of rapid transient growth. For example a barotropic flow setting and a perturbation wavelength corresponding to an almost neutral normal mode yielded a transient growth rate associated with "local" across ridge vortex interactions that was comparable in amplitude to the maximum value displayed in Fig. 1. Hence it is appropriate to regard the wave-train interaction effects, rendered transparent by the normal mode analysis, as indicative of the possible role of orographic slopes in the generation and interaction of a more limited number of cyclonic and anticyclonic perturbations.

4.3. Possible occurrence

The terrain-induced instability mechanism considered here is a feature of geostrophic/balanced flow dynamics. Thus in principle it could be engendered in any geophysical setting (limnological, oceanic, or atmospheric) that met the requisite conditions. In a limnological setting a surface wind stress that induced an anticyclonic shear across a sufficiently large and elongated lake could produce conditions favourable for the generation of the instability. Again Pedlosky (1980) suggested that eddies in the deep ocean might be attributable to the instability linked to terrain variations. Here we consider in more detail the possible occurrence of the instability in the atmosphere.

Elongated bands of enhanced lateral shear are a frequent feature of the atmosphere on the synoptic/sub-synoptic scale, and their characteristic amplitude betokens a growth rate comparable to, or in excess of, that associated with classical baroclinic instability. However two caveats are that a band needs to be co-aligned with a sufficiently elongated orographic ridge, and that the bands themselves occur predominantly within frontal regions of strong baroclinicity. The latter ingredient militates against the pure terrain instability but it can establish the hybrid configuration identified earlier. Thus, although pure terrain-induced instability can not be ruled out, it is more appropriate to focus on regions capable of manifesting the hybrid mode of terrain-related instability. Two examples of such regions are: the frequent alignment of a cold front along the eastern seaboard of north America providing, in conjunction with the Appalachian mountain chain in the hinterland, a west-to-east sequence of a positive terrain slope adjacent to a cold-to-warm thermal transition zone; the circumpolar flow around the margin of Antarctica, with the south-to-north sequence of the plateau to sea level slope, and the cold air mass over the extensive sea-ice giving away equatorward to warmer surface temperatures. Both regions are hence potentially the seat for the hybrid form of terrain instability if coupled with anticyclonic shear.

It is interesting to record that so-called "zipper-cyclones" accompany episodes of coastal front plus cold air damming along the Appalachian chain (see Keshishian and Bosart, 1987, and references therein), and also that cyclogenesis is

observed around the periphery of Antarctica (Mechoso, 1980; James, 1989; Carleton and Carpenter, 1990). In both cases, the systems tend be weak, shallow, synoptic/subsynoptic scale lows that propagate in the along-ridge/front direction, and moreover the systems often develop comparatively rapidly. These characteristics are all consistent with the results derived earlier.

5. Further remarks

The mechanism for, and the quintessential features of, a terrain-induced flow instability have been deduced by undertaking a normal mode analysis of an idealized quasi-geostrophic system and by invoking a phenomenological interpretation to account for the results. This groundwork provided a foundation for a discussion of the generality and limitations of the instability, and the possibility of its manifestation in various geophysical systems. In general the instability mechanism should be viewed as being merely indicative of the possible nature of terrain effects. However note was made of two locations where the atmospheric settings satisfy, to a large measure, the requirements for the instability and which are indeed regions of observed cyclogenetic activity.

REFERENCES

Blumsack, S. L. and Gierasch, P. J. 1972. Mars. The effect of topography on baroclinic instability. *J. Atmos. Sci. 29*, 1081–1089.

Carleton, A. M. and Carpenter, B. A. 1990. Satellite climatology of 'polar lows' and broadscale climatic associations for the southern hemisphere. *Intl. J. Climatol. 10*, 219–246.

Charney, J. G. and DeVore, J. G. 1979. Multiple flow equilibria in the atmosphere and blocking. *J. Atmos. Sci. 36*, 1205–1216.

Davies, H. C. 1975. Climatic change, orography and geostrophic motion. *Arch. Meteor. Geophys. Bioklim. B23*, 1–12.

Davies, H. C. and Horn, J. 1988. Semi-geostrophic flow of a stratified atmosphere over elongated isentropic valleys and ridges. *Tellus 40A*, 61–79.

DeSzoeke, R. A. 1975. Some effects of bottom topography on baroclinic instability. *J. Mar. Res. 33*, 93–122.

DeSzoeke, R. A. 1986. On the nonlinear evolution of baroclinic instability over topography. *Dyn. Atmos. Oceans. 10*, 221–2542.

Durney, B. R. 1977. The influence of mesoscale topography on the stability and growth rates of a two-layer model of the open ocean. *Geophys. Astrophys. Fluid Dyn. 9*, 115–128.

Frederiksen, J. S. and Bell, R. C. 1987. Teleconnection patterns and the roles of baroclinic, barotropic and topographic instability. *J. Atmos. Sci. 44*, 2200–2218.

Gill, A. E. 1974. The stability of planetary waves on an infinite beta-plane. *Geophys. Fluid Dyn. 6*, 29–47.

Hart, J. E. 1979. Barotropic quasi-geostrophic flow over anisotropic mountains. *J. Atmos. Sci. 36*, 1736–1746.

Hide, R. 1969. Some laboratory experiments on free thermal convection in a rotating fluid subject to a horizontal temperature gradient and their relation to the theory of the global atmospheric circulation. In: *The Global circulation of the atmosphere*, (ed. G. A. Corby). Roy. Met. Soc., London, 196–221.

Hoskins, B. J. 1973. Stability of the Rossby-Haurwitz wave. *Quart. J. Roy. Met. Soc. 99*, 723–745.

Hoskins, B. J., McIntyre, M. E. and Robertson, A. W. 1985. On the use and significance of potential vorticity charts. *Quart. J. Roy. Met. Soc. 111*, 877–946.

James, I. N. 1989. The Antarctic drainage flow: implications for hemispheric flow on the Southern Hemisphere. *Antarctic Science 1*, 279–290.

Källén, E. 1983. A note on orographically induced instabilities in two-layer models. *J. Atmos. Sci. 40*, 500–505.

Keshishian, L. and Bosart, L. F. 1987. A case study of extended east coast frontogenesis. *Mon. Wea. Rev. 115*, 100–117.

Lorenz, E. N. 1972. Barotropic instability of Rossby wave motion. *J. Atmos. Sci. 29*, 258–264.

Mechoso, C. R. 1980. The atmospheric circulation around Antarctica: linear stability and finite amplitude interactions with migrating cyclones. *J. Atmos. Sci. 37*, 2209–2233.

Mechoso, C. R. and Sinton, D. M. 1981. Instability of baroclinic flows with horizontal shear along topography. *J. Phys. Ocean. 11*, 813–821.

Orlanski, I. 1969. The influence of bottom topography on the stability of jets in a baroclinic fluid. *J. Atmos. Sci. 26*, 1216–1232.

Orlanski, I. and Cox, M. D. 1973. Baroclinic instability in ocean currents. *Geophys. Fluid Dyn. 4*, 297–332.

Pedlosky, J. 1980. The destabilization of shear flow by topography. *J. Phys. Ocean. 10*, 1877–1880.

Pedlosky, J. 1981. Resonant topographic waves in

barotropic and baroclinic flows. *J. Atmos. Sci. 38*, 2626–2641.

Reinhold, B. 1990. Orographic modulation of baroclinic instability. *J. Atmos. Sci. 47*, 1697–1713.

Revell, M. and Hoskins, B. J. 1984. Orographically induced Rossby wave instabilities. *J. Atmos. Sci. 41*, 51–67.

Schär, Ch. and Davies, H. C. 1990. An instability of mature cold fronts. *J. Atmos. Sci. 47*, 929–950.

Speranza, A., Buzzi, A., Trevisan, A. and Malguzzi, P. 1985. A theory of deep cyclogenesis in the lee of the Alps. Part I: modifications of baroclinic instability by localised topography. *J. Atmos. Sci. 42*, 1521–1535.

Thorsteinsson, S. 1988. Finite amplitude stratified flow past isolated mountains on an f-plane. *Tellus 40A*, 220–236.